A&A 633, A44 (2020)
https://doi.org/10.1051/0004-6361/201936038

Astronomy & Astrophysics

A HARPS RV search for planets around young nearby stars*

A. Grandjean[1], A.-M. Lagrange[1], M. Keppler[2], N. Meunier[1], L. Mignon[1], S. Borgniet[3], G. Chauvin[1], S. Desidera[4], F. Galland[1], S. Messina[5], M. Sterzik[6], B. Pantoja[7], L. Rodet[1], and N. Zicher[8]

[1] Univ. Grenoble Alpes, CNRS, IPAG, 38000 Grenoble, France
e-mail: antoine.grandjean1@univ-grenoble-alpes.fr
[2] Max Planck Institute for Astronomy, Königstuhl 17, 69117 Heidelberg, Germany
[3] CNRS Lesia (UMR8109) – Observatoire de Paris, Paris, France
[4] INAF – Osservatorio Astronomico di Padova, Vicolo dell'Osservatorio 5, Padova 35122, Italy
[5] INAF – Osservatorio Astrofisico di Catania, via Santa Sofia, 78 Catania, Italy
[6] European Southern Observatory (ESO), Alonso de Córdova 3107, Vitacura, Casilla 19001, Santiago, Chile
[7] Departamento de Astronomía, Universidad de Chile, Camino al Observatorio, Cerro Calán, Santiago, Chile
[8] Oxford Astrophysics, Department of Physics, Denys Wilkinson Building, UK

Received 6 June 2019 / Accepted 14 October 2019

ABSTRACT

Context. Young nearby stars are good candidates in the search for planets with both radial velocity (RV) and direct imaging techniques. This, in turn, allows for the computation of the giant planet occurrence rates at all separations. The RV search around young stars is a challenge as they are generally faster rotators than older stars of similar spectral types and they exhibit signatures of magnetic activity (spots) or pulsation in their RV time series. Specific analyses are necessary to characterize, and possibly correct for, this activity.
Aims. Our aim is to search for planets around young nearby stars and to estimate the giant planet (GP) occurrence rates for periods up to 1000 days.
Methods. We used the HARPS spectrograph on the 3.6 m telescope at La Silla Observatory to observe 89 $A-M$ young (<600 Myr) stars. We used our SAFIR (Spectroscopic data via Analysis of the Fourier Interspectrum Radial velocities) software to compute the RV and other spectroscopic observables. Then, we computed the companion occurrence rates on this sample.
Results. We confirm the binary nature of HD 177171, HD 181321 and HD 186704. We report the detection of a close low mass stellar companion for HIP 36985. No planetary companion was detected. We obtain upper limits on the GP (<13 $M_{\rm Jup}$) and BD ($\in$ [13; 80] $M_{\rm Jup}$) occurrence rates based on 83 young stars for periods less than 1000 days, which are set, 2^{+3}_{-2} and 1^{+3}_{-1}%.

Key words. techniques: radial velocities – stars: activity – binaries: spectroscopic – planetary systems – starspots – stars: variables: general

1. Introduction

More than four thousand exoplanets have been confirmed and most of them have been found by transit or radial velocity (RV) techniques[1]. The latter, although very powerful, is limited by the parent star's activity (spots, plages, convection, and pulsations). Young stars are generally faster rotators than their older counterparts (Stauffer et al. 2016; Rebull et al. 2016; Gallet & Bouvier 2015). They can also exhibit activity-induced RV jitter with amplitudes up to 1 km s^{-1} (Lagrange et al. 2013), larger than the planet's induced signal. False positive detections have been reported around young stars in the past (Huélamo et al. 2008; Figueira et al. 2010; Soto et al. 2015).

We have carried out an RV survey to search for planets around such young stars with the High Accuracy Radial velocity Planet Searcher (HARPS; Mayor et al. 2003) and SOPHIE (Bouchy & Sophie Team 2006) spectrographs with the final aim of coupling RV data with direct imaging (DI) data, which will allow for the computation of detection limits, for each targets at all separations and then to compute occurrences rates for all separations. A feasibility study was carried out by Lagrange et al. (2013) on 26 stars of the survey with HARPS, demonstrating that we can probe for giant planets (1–13 $M_{\rm Jup}$, hereafter GP) with semi-major axis up to 2 au and couple the survey data with direct imaging data. The time baseline of our survey also permits a probe of the hot Jupiter (hereafter HJ) domain around young stars. Although GP formation models predict a formation at a few au (Pollack et al. 1996), migration through disc-planet interaction (Kley & Nelson 2012) or gravitational interaction with a third body can allow the planet to finally orbit close to the star (Teyssandier et al. 2019). HJ are common among exoplanets orbiting older main sequence stars as they represent one detected planet out of five (Wright et al. 2012). While previous RV surveys on small sets of young stars showed no evidence for the presence of young HJ (Esposito et al. 2006; Paulson & Yelda 2006), two HJ around young stars were recently discovered by Donati et al. (2016) and Yu et al. (2017). However, we still need to find out if this kind of object is common at young age or not and we need to compare the migration models with observations in order to constrain the migration timescales.

Here, we report on the results of our large HARPS survey. We describe our survey sample and observations in Sect. 2. In Sect. 3, we focus on GP, brown dwarf (BD), and stellar

* A table of the radial velocities is only available at the CDS via anonymous ftp to cdsarc.u-strasbg.fr (130.79.128.5) or via http://cdsarc.u-strasbg.fr/viz-bin/cat/J/A+A/633/A44
[1] exoplanet.eu

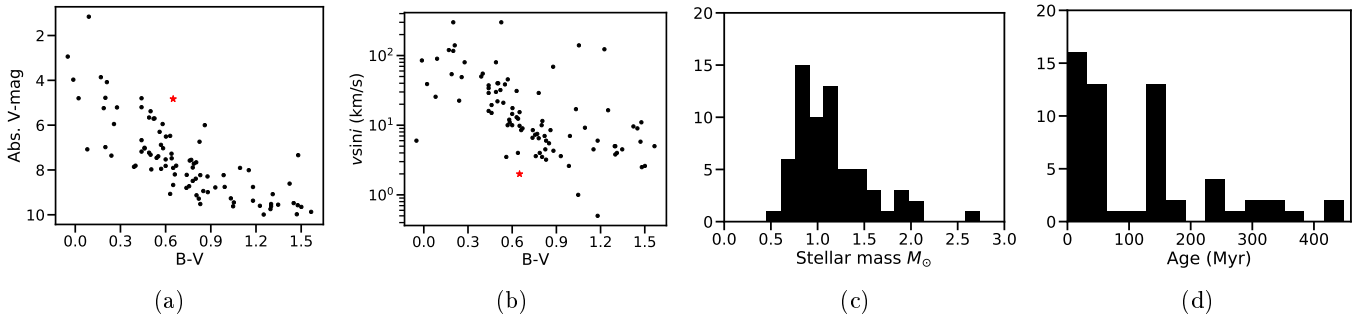

Fig. 1. Main physical properties of our sample. (*a*) Absolute V-magnitude vs. $B-V$. Each black dot corresponds to one target. The Sun is displayed (red star) for comparison. (*b*) $v \sin i$ vs $B-V$ distribution. (*c*) Mass histogram (in $M_\odot$). (*d*) Age histogram.

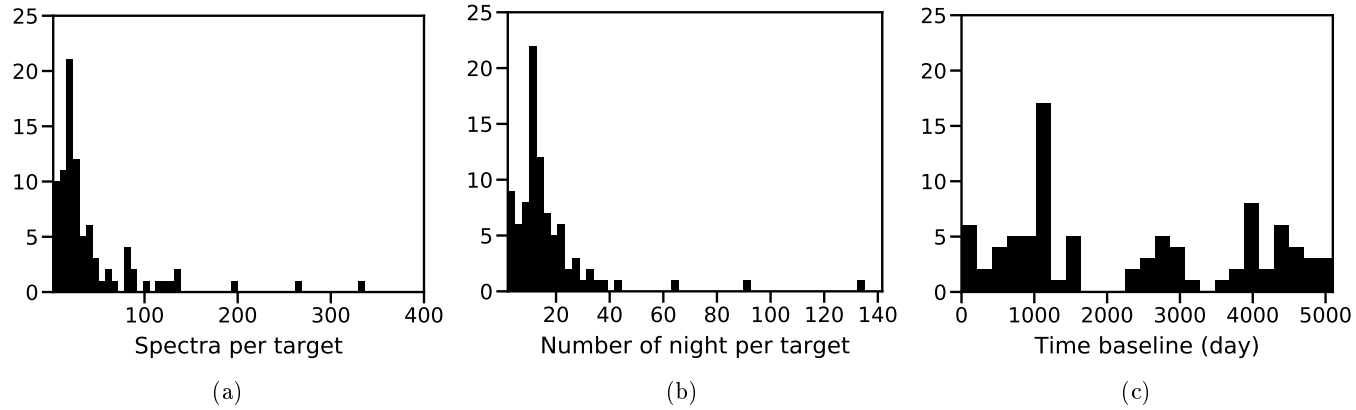

Fig. 2. Observation summary. (*a*) Histogram of the number of spectra per target, excluding HD 216956 (Fomalhaut, 834 spectra) and HD 039060 (β Pic, 5108 spectra). (*b*) Histogram of the number of nights per target. (*c*) Histogram of the time baselines.

companions detections. In Sect. 4, we perform a statistical analysis of our sample and compute the close GP and BD occurrence rates around young stars. We conclude our findings in Sect. 5.

2. Description of the survey

2.1. Sample

We selected a sample of 89 stars, chosen to their brightness ($V < 10$), ages as fund in the literature (<300 Myr for most of them, see Table A.1), and distance (<80 pc) determined from their HIPPARCOS parallaxes (van Leeuwen 2007). These criteria ensure we will get the best detection limits for both the HARPS RV and SPHERE DI surveys at, respectively, short (typically 2−5 au), and large (further than typically 5 au) separations. Indeed, observing bright stars allow us to obtain spectra with a better signal-to-noise ratio (S/N). Moreover, young planets are still warm from their formation and are then brighter, which lowers the contrast between them and their host stars, while short distances allow for better angular resolutions in direct imaging. Most of the targets are part of the SPHERE GTO The SpHere INfrared survey for Exoplanets (SHINE) survey sample (Chauvin et al. 2017a). Binary stars with an angular separation on the sky that is lower than 2 as were not selected to avoid contamination in the spectra from the companion

Their spectral types range from A0V to M5V (Fig. 1). Their projected rotational velocity ($v \sin i$) range from 0.5 to 300 km s^{-1} with a median of 11 km s^{-1}, their V-band magnitude are mainly between 4 and 10 with a median of 7.8. Their masses are between 0.6 and 2.74 $M_\odot$ with median of 1.07 $M_\odot$. Our sample includes 26 targets between A0 and F5V ($B-V \in [-0.05 : 0.52]$), 55 between F6 and K5 ($B-V \in [-0.05 : 0.52]$), and 8 between K6 and M5 ($B-V \geq 1.33$). Noticeably, our sample includes stars with imaged planetary or substellar companions (among them β Pic, AB Pic, HN Peg, GJ 504, HR 8799, HD 95086, HD 106906 or PZ Tel). We present the main characteristics of our star sample in Fig. 1 and Table A.1.

2.2. Observations

We observed our 89 targets mainly between 2013 and 2016. Some stars were part of previous surveys by Borgniet et al. (2017) and Lagrange et al. (2009a), which allows us to reach a time baseline up to 10 yr. Some stars had already been observed with HARPS before, some since the HARPS commissioning in 2003. Additional observations were also obtained in October 2017, December 2017, and March 2018.

We use the observing strategy described in Borgniet et al. (2017), which consist of recording two spectra per visit and to observe each target on several consecutive nights to have a good sampling of the short-term jitter. The median time baseline is 1639 days (mean time baseline of 2324 days), with a median number of spectra per target of 25 (52 on average) spaced on a median number of 12 nights (17 on average, Fig. 2). Details can be found in Table A.1.

2.3. Observables

From the HARPS spectra we derived the RV and whenever possible the cross-correlation function (CCF), bisector velocity span (hereafter BVS), and $\log R'_{\rm HK}$ with our SAFIR software for Spectroscopic data via Analysis of the Fourier Interspectrum Radial

velocities. It builds a reference spectrum from the median of all spectra available on a given star and computes the relative RV in the Fourier plane. The computed RV are then relative to the reference spectrum. The efficiency of this method was proved in the search of companions (Galland et al. 2005a,b). We mainly use the correlation between RV and BVS to determine the main source of RV variability: magnetic activity, pulsations or companions (Lagrange et al. 2009a; Borgniet et al. 2017). We excluded spectra with S/N at 550 nm which was too high (>380), to avoid saturation or too low (<80), to avoid bad data, as well as spectra with an air mass that was too high (sec $z > 3$), and spectra that were too different from the reference spectrum of the star ($\chi^2 > 10$). For M-type stars, we used a lower limit of 40 in S/N at 550 nm as it is a better compromise for these stars to provide enough spectra to perform our analysis without including bad spectra.

3. Detected companions in the HARPS survey

3.1. Long period companions, RV long-term trends, and stellar binaries

In this section we describe the stars for which we identified a GP companion with a period higher than 1000 days, a long-term trend RV signal or a binary signal. When possible, we characterize the companion using the *yorbit* software that fits RV with a sum of Keplerian or a sum of keplerians plus a drift (Ségransan et al. 2011).

3.1.1. HD 39060

β Pic is an A6V pulsating star that hosts an imaged edge-on debris (Smith & Terrile 1984) and gas disk (Hobbs et al. 1985), and an imaged GP at 9 au (Lagrange et al. 2009b, 2019a). This star presents also exocomets signatures in its spectra (Lagrange-Henri et al. 1988; Beust et al. 1989; Kiefer et al. 2014). β Pic was observed with HARPS since its commissioning in 2003, totalizing more than 6000 spectra with a mean S/N at 550 nm of 273. Until 2008, spectra were taken to study the Ca II absorption lines associated to the falling exocomets. Since 2008, we adopted a specific observation strategy, to properly sample the stellar pulsations and to correct the RV from them, (Lagrange et al. 2012, 2019b). It consisted in observing the star for continuous sequences of 1−2 h. Longer sequences up to 6h were obtained in 2017−2018. This allowed to detect a new GP companion within the pulsations signal of β Pic. The discovery of this 10 $M_{\rm Jup}$, 1200 days period companion is detailed in Lagrange et al. (2019b).

3.1.2. HD 106906

HD 106906 is a F5V star in the Sco-Cen young association. Bailey et al. (2014) Imaged a giant planet companion at 7.1 as (650 au) in 2014. HARPS data from this survey together with the PIONER interferometer data allowed to detect a close low mass stellar companion to HD 106906 with a period of 10 days, (Lagrange et al. 2015). The presence of the binary could explain the wide orbit of HD 106906b under some circumstances (Rodet et al. 2017).

3.1.3. HD 131399

HD 131399 is member of a complex hierarchical system. HD 131399A forms a binary with the tight binary HD 131399BC.

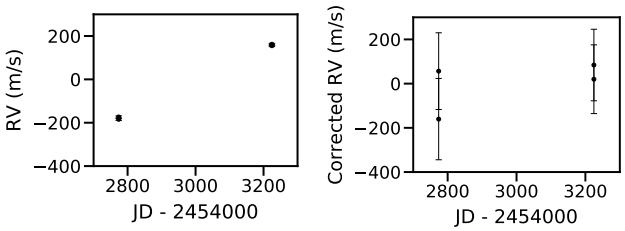

Fig. 3. HD 186704 RV long term trend. *Left*: RV time variations, *right*: RV corrected from the RV-BVS correlation time variations.

A GP companion was discovered with SPHERE around HD 131399A by Wagner et al. (2016) but is now identified as a background star with similar proper motion (Nielsen et al. 2017). We detected in this survey the presence of a close stellar companion to HD 131399A, with a period of 10 days (0.1 au), and an $M \sin i$ of 450 $M_{\rm Jup}$ (Lagrange et al. 2017).

3.1.4. HD 177171

HD 177 171 (ρ Tel) was reported as a spectroscopic binary by Nordström et al. (2004) and as an astrometric binary by Frankowski & Jorissen (2007) from the HIPPARCOS data. This is confirmed by Lagrange et al. (2013) in the feasibility study of this survey. We measure an amplitude of at least 20 km s^{-1} in the RV. Our time sampling does not allow for the estimation the period of this stellar companion.

3.1.5. HD 186704A

HD 186704 is a known binary system with a companion at 10 as (Zuckerman et al. 2013). Nidever et al. (2002) report a trend in the RV of 88 ± 8 ms^{-1} d^{-1} with a negative curvature based on 4 observations spaced on 70 days for HD 186704AB. Tremko et al. (2010) observe a change in the RV of 4200 ms^{-1} in 8682 days on HD 186704A. Finally, Tokovinin (2014) reporte HD 186704A as hosting a spectroscopic binary (SB) companion with a 3990 days period. We observe a trend of 340 ms^{-1} over a duration of 450 days in the RV of HD 186704A based on 4 spectra. This corresponds to a slope of 0.75 ms^{-1} d^{-1}. The star present signs of activity, we therefore corrected the RV using the RV-BVS correlation using Melo et al. (2007) method (see Appendix B). The trend is still visible with a lower slope 0.23 ms^{-1} d^{-1}. We present the RV and corrected RV of HD 186704A in Fig. 3. The difference of one order of magnitude on the slope of the trend between Nidever et al. (2002) observations and ours can be explained by the fact that our observations were made when the SB was closer to the periastron or apoastron of its orbit.

3.1.6. HD 181321

We confirm that HD 181321 is an SB. Nordström et al. (2004) report a variation of 2.3 km s^{-1} over 9 yr, Guenther & Esposito (2007) report a trend with a slope of 1.4 km s^{-1} yr^{-1}. Our observations spread on 3757 days (10.3 yr) cover at least two orbital periods. The star is active and show BVS variations with a period of 2−2.5 days that should correspond to the rotational period of the star. We use *yorbit* to fit the RV with two Keplerian models, one to fit the stellar activity variation and an another to fit the binary variations. We find two possible solutions for the companion, one with a period of 1600 days (2.7 au) and a minimum mass of 0.1 $M_{\odot}$, and a second with a period of 3200 days (4.4 au)

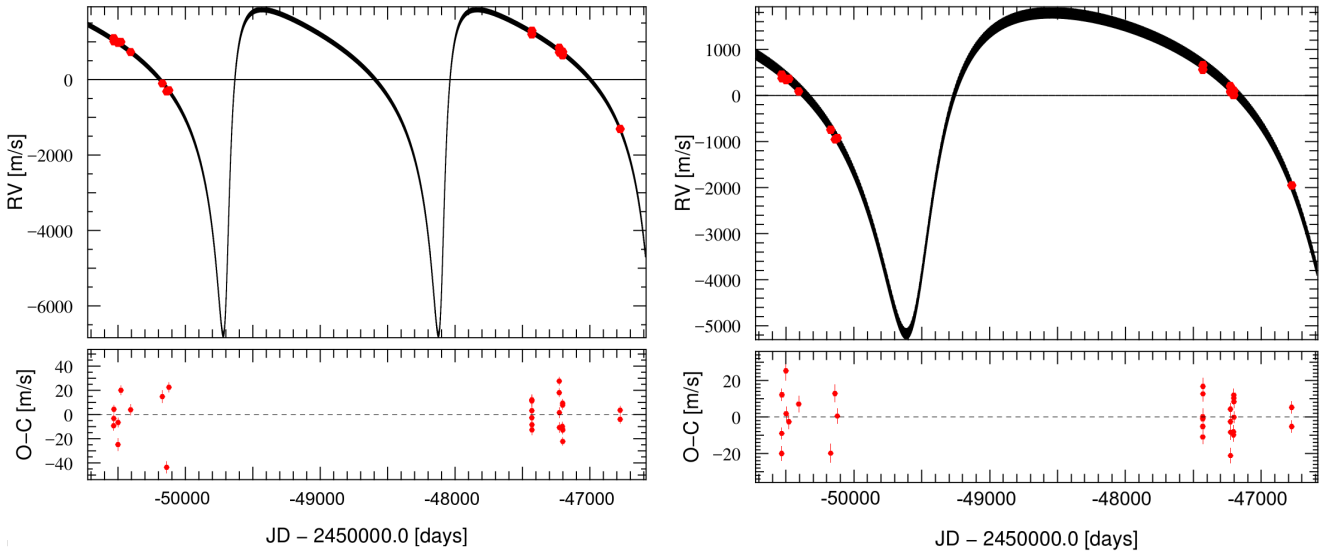

Fig. 4. Solutions of HD 181321 RV fit by the sum of two Keplerian (*top*) and their residuals (*bottom*). *Left*: 1600 days solution. *Right*: 3200 days solution.

and a minimum mass of 0.18 $M_{\odot}$. In both cases, the eccentricity is ∼0.5. We present those two solutions in Fig. 4. More data are needed in order to distinguish between those two solutions.

3.1.7. HD 206893

HD 206893 is a F5V star that hosts a directly imaged BD companion at a separation of 270 mas (Milli et al. 2017; Delorme et al. 2017). We recently reported in Grandjean et al. (2019) a long-term trend in the star RV coupled with pulsations with periods slightly less than one day. We performed an MCMC on both the RV trend, imaging data, and HIPPARCOS-*Gaia* proper motion measurements to constrain the orbit and dynamical mass of the BD. We concluded that the trend can not be attributed to the BD as it leads to dynamical masses incompatible with the object's spectra. The presence of an inner companion that contributes significantly to the RV trend is suggested with a mass of 15 $M_{\rm Jup}$, and a period between 1.6 and 4 yr.

3.1.8. HD 217987

HD 217987 is a M 2V, high proper motion star and exhibits a long-term RV trend induced by its secular acceleration. We therefore corrected the RV from the star secular acceleration in its proper motion we deduced from its paralax and proper motion reported in Gaia Collaboration (2018) (see Fig. 5). The corrected RV presents short period variations. The RV and BVS are correlated which indicate that the signal might be dominated by spots or plages (see Fig. 5). We observe a long-term variation in $\log R'_{\rm HK}$, FWHM, and RV which are better fitted by a second degree polynomial model than with a linear model (see Fig. 5). This variation could be then attributed to a magnetic cycle of the star with a period greater than 5000 days. An analysis on a large number of M dwarf was made by Mignon et al. (in prep.), including this star and we should expect an offset of approximately $-10\,{\rm ms}^{-1}$ in the RV due to the HARPS fiber change of the 15th of June 2015 for this star. We observe an offset in the star's BVS at this date date (see Fig. 5), but no significant offset in the RV. We use one template on all the data (see Sect. 2.3), the impact of the HARPS fiber change is then averaged. This can explain why we do not see a significant RV offset for this star.

3.1.9. HIP 36985

HIP 36985 is a M 2V-type star reported as a wide binary with the system GJ 282AB at a separation of 1.″09 (Poveda et al. 2009). We observe an RV long-term variation with an amplitude of 700 $\rm ms^{-1}$ on a time baseline of 1400 days in addition to a short-term variation with an amplitude of 50 $\rm ms^{-1}$. No correlation between RV and BVS is seen, which excludes stellar activity or pulsations as the origin of the long-term variations. The mean $\log R'_{\rm HK}$ of our spectra of −4.3 indicates that the short-term variations come from magnetic activity (spots). We fit the RV with *yorbit* using two Keplerian models, one to fit the long-term variations and an another to fit the companion variations. We present our best solution in Fig. 6 and the corresponding companion parameters in Table 1. The companion minimum mass deduced from the present data is 29 $M_{\rm Jup}$ and the period is 8400 days (23 yr), corresponding to a semi-major axis of 7 au and a projected separation of 497 mas. We observed HIP 36985 with SPHERE in 2018 and confirm the presence of a however low-mass star companion (Biller et al., in prep.). We find a period of 22 days for the short-term variations, while the rotation period is of 12 ± 0.1 days (Díez Alonso et al. 2019). The poor sampling of those short-term variations probably explains the strong difference with the rotation period.

3.2. Giant planets

No giant planet companion of period less than 1000 days is detected. In addition to the stars presented in Sect. 3, some stars presented RV variations without a significant correlation between RV and BVS. For these stars we compared the RV periodogram with the BVS periodogram and the time window periodogram. In all cases, putative periods associated with the RV were also present in the BVS or time window periodograms, or in both. This implies that these RV variations are most likely due to stellar activity or pulsations. We present as an example BD+20 2465 in Fig. 7. This star shows RV variations with

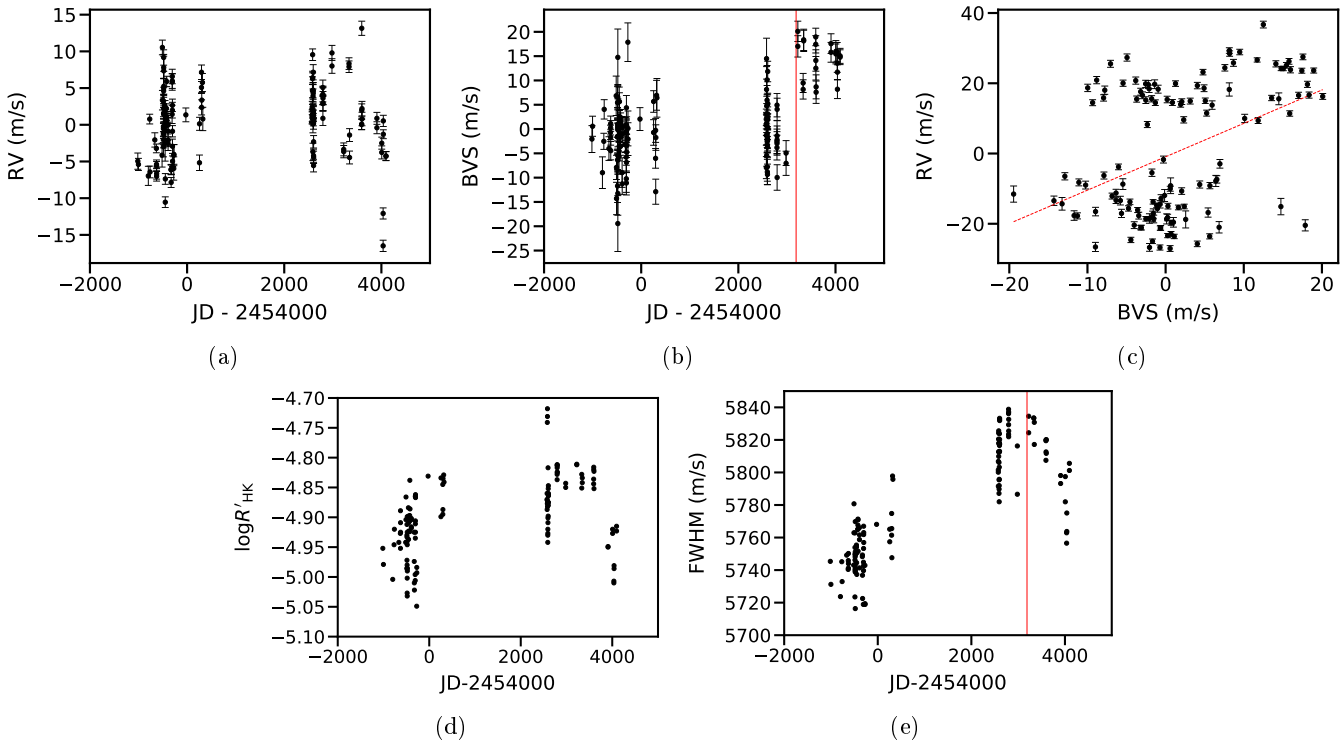

Fig. 5. HD 217987 summary. (*a*) RV time variations corrected from the secular acceleration drift. (*b*) BVS time variations, HARPS fiber change is shown with a vertical red line. (*c*) RV corrected from the secular acceleration drift vs BVS. The best linear fit is presentend in red dashed line. (*d*) $\log R'_{HK}$ time variations. (*e*) FWHM time variations.

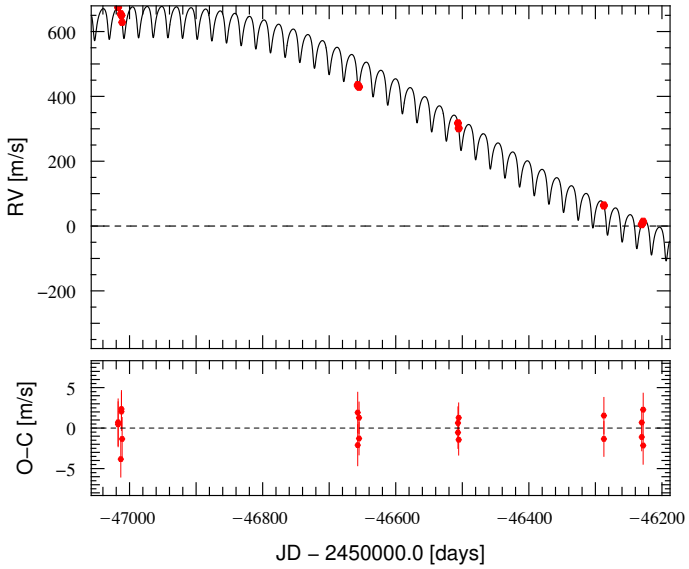

Fig. 6. Solution of HIP 36985 RV's fit by a sum of two keplerians and its residuals

periods near 2 days which are both present in the time window periodogram and BVS periodogram.

4. Analysis

4.1. Stellar intrinsic variability

Figure 8 displays the mean RV uncertainty vs. $B-V$, $v \sin i$ and M_*. We also display the RV rms vs. $B-V$, and age in Fig. 9. We observe that the mean RV uncertainty is correlated to the $v \sin i$

Table 1. HIP 36985B's orbital parameters.

Parameters	Value
P (days)	8500^{+1900}_{-1900}
a (au)	$7^{+1}_{-1.1}$
Separation (mas)	500^{+70}_{-80}
e	0.55 ± 0.04
ω (°)	50 ± 67
K (ms^{-1})	480 ± 230
$M \sin i$ (M_{Jup})	29^{+18}_{-16}

(Pearson = −0.65, $p_{value} \ll 1\%$). This is consistent with what is observed on older, AF main sequence stars by Borgniet et al. (2017, 2019). We observe a strong jitter for most of the stars. The ratio between RV rms and the mean RV uncertainty is between 390 and 1 with a median at 16.

The median RV rms is 49 ms^{-1} (300 ms^{-1} on average). This jitter is mainly caused by pulsations for early type stars (from A to F5V), and by spots and faculae for late type stars (>F5V). Those two regimes can be distinguished, as stars with pulsations shows a vertical spread of BVS(RV) diagram, whereas stars with spots present a correlation between RV and BVS (Lagrange et al. 2009a). The main origin of RV jitter is reported in Table A.2 for each target.

78 stars out of 89 of our sample present variations in their Ca lines. The median $\log R'_{HK}$ of our sample is −4.3 with a standard deviation of 0.2. 4 stars present signs of low activity ($\log R'_{HK} < -4.75$), 59 are active ($-4.75 < \log R'_{HK} < -4.2$) and 15 stars present signs of high activity ($\log R'_{HK} > -4.2$). We

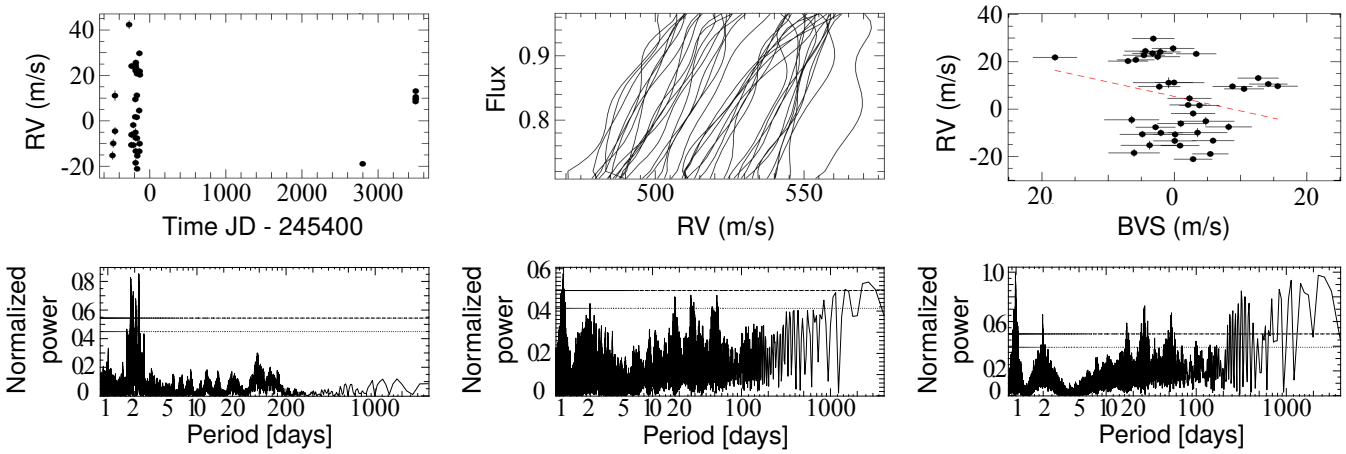

Fig. 7. BD+20 2465 summary. *Top row*: RV time variations, *left*: bisectors, *middle*: RV vs BVS (*right*). *Bottom row*: RV periodogram (*left*), BVS periodogram (*middle*), time window peridogram (*right*). The FAP at 1 and 10% are presented respectively in dashed lines and in dotted lines.

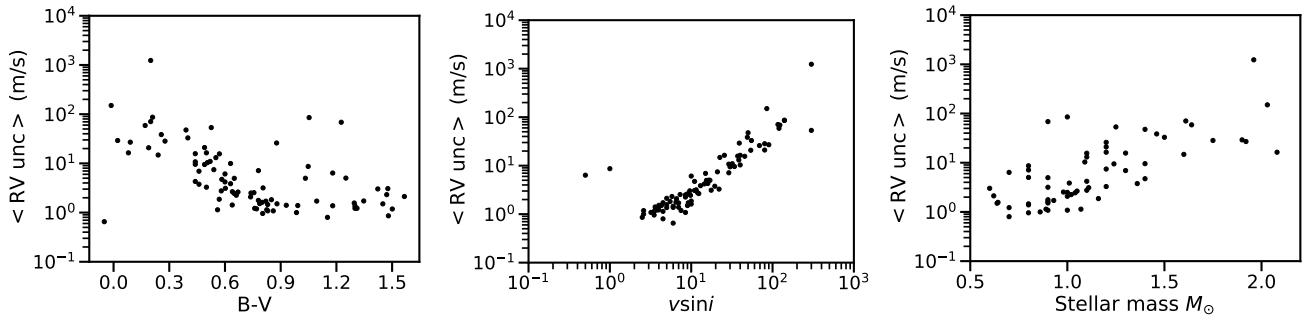

Fig. 8. Summary of the survey RV uncertainties. Mean RV uncertainty (accounting for the photon noise only) vs. $B-V$ (*left*), vs. $v \sin i$ (*middle*) and vs. $M_\star$ (in $M_\odot$, *right*).

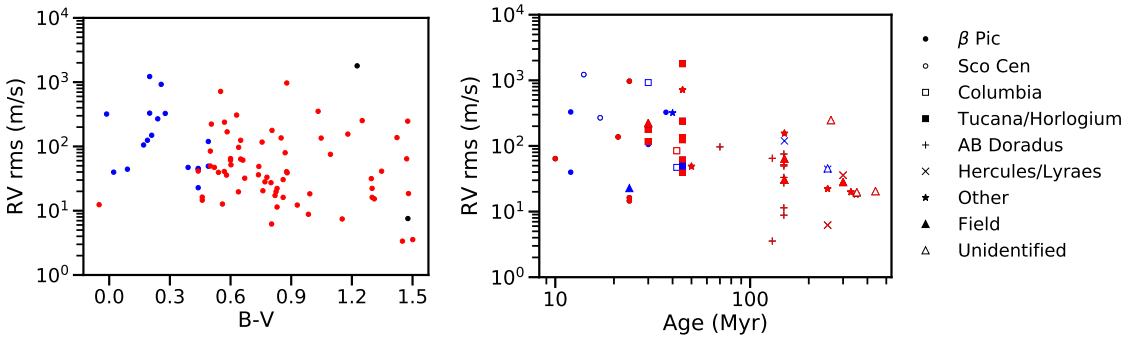

Fig. 9. Survey RV rms summary. *Left*: RV rms vs. $B-V$, *right*: RV rms and vs. age. Pulsating stars are plotted in blue, stars with RV dominated magnetic activity (spots) are plotted in red and stars with undetermined main source of RV are plotted in black. Stars with SB signature are not displayed (HD 106906, HD 131399, HD 177171). HD 197890 is not considered due to a too small set of data available.

present in Fig. 10 $\log R'_{\rm HK}$ vs. $B-V$. Some early F-type pulsating stars also present signs of actity when all late type stars present signs of activity.

4.2. HARPS fiber change

In June 2015, the fiber of the HARPS instrument was changed in order to increase its stability (Lo Curto et al. 2015). Lo Curto et al. (2015) show that it leads to a change in the instrument profile which impacts the CCF computation and therefore the RV and BVS computation. They observed an offset in the RV between the datasets taken before and after this change of the order of 15 $\rm ms^{-1}$ for old F to K-type stars, based on 19 stars (Lo Curto et al. 2015). A more detailed analysis is currently underway for a large sample of close M-type main sequence stars (Mignon et al., in prep.). In this analysis, two reference spectra are computed, one before the change and one after. Our current set of spectra for each star is not big enough to build reference spectra as done in Mignon et al. (in prep.). The offset is different from one star to the other and its correlation with stellar parameters is not yet determined (spectral type, $v \sin i$ etc.). This offset has not been estimated on young stars before and the impact of high $v \sin i$ and strong jitter is not known. One should be careful before trying to correct this offset in order to not remove signal.

The difference between the mean of the RV before and after the fiber change can be measured, however, it won't probe the

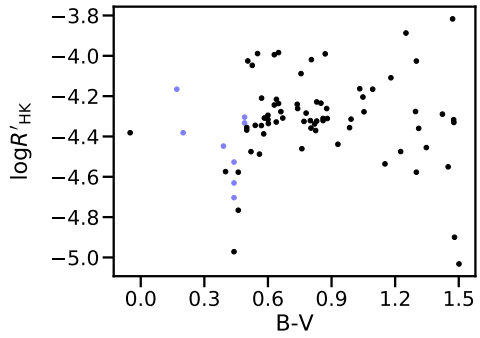

Fig. 10. Survey $\log R'_{\rm HK}$ vs. $B-V$. Pulsating stars are plotted in blue.

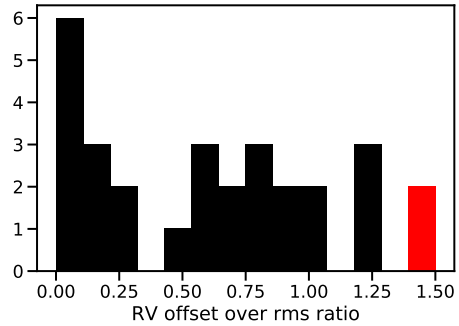

Fig. 11. Histogram of the ratio between the difference in the RV mean between before and after HARPS' fiber change, and the maximum of the rms before and after the fiber change. The stars that present a ratio greater than 1.3 are plotted in red.

offset alone, as long-term variations (star magnetic cycle, unseen companions, etc.) or a bad sampling of the jitter can also induce a difference in the mean of the RV.

We then decided to correct the offset only when it is significant enough. We compared the difference between the RV mean before and after the fiber change to the maximum of the rms before and after the fiber change to determine it. First, we selected the stars for which computing rms before and after the fiber change is relevant: we excluded the stars for which we have less than 10 spectra, less than 6 spectra before the fiber change, and less than 6 spectra after. We excluded the stars identified as SB (marked "B" in Table A.2) or presenting a long-term variation due to a companion (marked "T" in Table A.2). We also excluded the stars for which the RV amplitude is more than 900 $\rm ms^{-1}$ as the offset should be negligible compared to the jitter. We finally excluded HD 169178 that presents a trend due to a magnetic cycle. Finally, 29 stars were not excluded. We present the histogram of the ratio between the difference in mean of RV between before and after the fiber change and the maximum of the rms before and after the fiber change in Fig. 11. We chose to correct the RV offset for the stars that present a ratio larger than 1.3 a threshold that ensure a significant offset. Two stars correspond to this criterion. We present the characteristics of their offset in Table 2, and we present the correction of the offset for one of them in Fig. B.2. They have G to K-types and present an offset of the order of 50 $\rm ms^{-1}$. Such offsets are three times larger than those founds on old stars (Lo Curto et al. 2015).

4.3. Exclusion of peculiar stars and RV correction for further analysis

In order to better estimate the number of potentially missed planets in our survey, we excluded some stars from our analyze and made some corrections on others before computing the detection limits. We excluded SB stars (HD 106906, HD 131399, HD 177171, HD 181321). Further, we excluded HD 116434 since its high value of $v \sin i$ (>200 $\rm km\,s^{-1}$) prevents the measurements of BVS. We also excluded HD 197890 for which our data are too sparse to reliably quantify the detection limits (3 spectra). Thus leads to 83 stars, 23 A-F stars, 52 F-K stars, and 8 K-M stars.

For stars with RV dominated by spots (marked A in the Table A.2) we corrected their RV from the RV-BVS correlation using Melo et al. (2007) method (see Appendix B). We corrected HD 217987 RV from its proper motion and HD 186704 RV from its long-term trend with a linear regression. For β Pic, we considered the RV corrected from its pulsations as well as β Pic b and c contributions (Lagrange et al. 2019b).

For the stars for which we identified a non ambiguous offset in the RV, we corrected their RV from this offset (see Table 2).

Table 2. Parameters of the stars that present a significant offset.

Name	ST	$B-V$	$\langle FWHM \rangle$ ($\rm km\,s^{-1}$)	Offset ($\rm ms^{-1}$)	Ratio
HD 7661	K0V	0.77	9.2	42	1.4
HD 218860	G8V	0.74	11.7	57	1.4

Notes. The offset is the difference between the RV mean before and after HARPS' fiber change, and the ratio is the ratio between the offset and the maximum of the rms before and after the fiber change.

4.4. Detection limits

We compute $m_p \sin i$ detection limits for periods between 1 and 1000 days in the GP domain (between 1 and 13$M_{\rm Jup}$), and in the BD domain (between 13 and 80 $M_{\rm Jup}$). We use the Local Power Analysis (LPA; Meunier et al. 2012; Borgniet et al. 2017) which determines, for all periods P, the minimum $m_p \sin i$ for which a companion on a circular orbit with a period P would lead to a signal consistent with the data, by comparing the synthetic companion maximum power of its periodogram to the maximum power of the data periodogram within a small period range around the period P.

We then compute the completeness function $C(m_p \sin i, P)$ which corresponds for a given couple $(m_p \sin i, P)$ to the fraction of stars for which the companion is excluded by the detection limits (Borgniet et al. 2017). We present the 40–80% search completeness in Fig. 12.

4.5. Companion occurrence rates

We compute the upper limits of companions occurrence rates for our 83 stars in the GP (1–13 $M_{\rm Jup}$) and BD (13–80 $M_{\rm Jup}$) domains for AF ($B-V \in [-0.05: 0.52]$), FK ($B-V \in [0.52: 1.33]$), KM ($B-V \geq 1.33$) type stars for different ranges of periods: 1–10, 10–100, 100–1000, and 1–1000 days. We use the method described in Borgniet et al. (2017) to compute the occurrence rates and to correct them from the estimated number of missed companions $n_{\rm miss}$ derived from the search completeness.

We present the upper limits of the occurrence rates for all stars in Fig. 13 and for AF, FK, M, and all stars in Table 3. The GP occurrence rate is below 2^{+3}_{-2}% (1σ) and the BD occurrence rate is below 1^{+3}_{-1}% (1σ) for periods under 1000 days.

Table 3. GP ($m_p \sin i \in [1, 13]$ $M_{\rm Jup}$) and BD ($m_p \sin i \in [13, 80]$ $M_{\rm Jup}$) occurrence rates around young nearby stars.

$m_p \sin i$ interval ($M_{\rm Jup}$)	Orbital period interval (day)	$B-V$	Search completeness C (%)	Detected GP systems	Missed GP systems **upper limit**	GP occurrence rate upper limit (%)	Confidence intervals 1σ (%)	Confidence intervals 2σ (%)
1–13	1–10	All	94	0	0.1	1.3	0–4.1	0–7.0
(GP)		[−0.05 : 0.52]	**89**	**0**	**0.1**	**4.9**	**0–14.7**	**0–24.0**
		[0.52 : 1.33]	*95*	*0*	*0.1*	*2.0*	*0–6.4*	*0–10.8*
		≥1.33	***98***	***0***	***0.0***	***12.8***	***0–32.9***	***0–50.0***
	1–100	All	89	0	0.1	1.4	0–4.4	0–7.4
		[−0.05 : 0.52]	**81**	**0**	**0.2**	**5.4**	**0–16.3**	**0–26.7**
		[0.52 : 1.33]	*91*	*0*	*0.1*	*2.1*	*0–6.7*	*0–11.3*
		≥1.33	***92***	***0.1***	***0.0***	***13.6***	***0–35.0***	***0–53.1***
	1–1000	All	80	0	0.3	1.5	0–4.9	0–8.3
		[−0.05 : 0.52]	**71**	**0**	**0.4**	**6.2**	**0–18.6**	**0–30.5**
		[0.52 : 1.33]	*82*	*0*	*0.2*	*2.4*	*0–7.5*	*0–12.6*
		≥1.33	***86***	***0***	***0.2***	***14.5***	***0–37.4***	***0–56.6***
13–80	1–10	All	99	0	0.0	1.2	0–3.9	0–6.6
(BD)		[−0.05 : 0.52]	**99**	**0**	**0.0**	**4.4**	**0–13.2**	**0–21.6**
		[0.52 : 1.33]	*99*	*0*	*0.0*	*1.9*	*0–6.2*	*0–10.4*
		≥1.33	***99***	***0***	***0.0***	***12.6***	***0–32.6***	***0–49.5***
	1–100	All	97	0	0.0	1.2	0–4.0	0–6.8
		[−0.05 : 0.52]	**95**	**0**	**0.0**	**4.6**	**0–13.7**	**0–22.5**
		[0.52 : 1.33]	*97*	*0*	*0.0*	*2.0*	*0–6.3*	*0–10.6*
		≥1.33	***93***	***0***	***0.1***	***13.4***	***0–34.7***	***0–52.6***
	1–1000	All	92	0	0.1	1.3	0–4.2	0–7.2
		[−0.05 : 0.52]	**89**	**0**	**0.1**	**4.9**	**0–14.7**	**0–24.0**
		[0.52 : 1.33]	*93*	*0*	*0.1*	*2.1*	*0–6.6*	*0–11.1*
		≥1.33	***90***	***0***	***0.1***	***13.8***	***0–35.7***	***0–54.1***

Notes. The parameters are displayed in normal, bold, italic or bold and italic fonts when considering the full star sample, the early type AF stars, FK-type stars or KM-type stars, respectively.

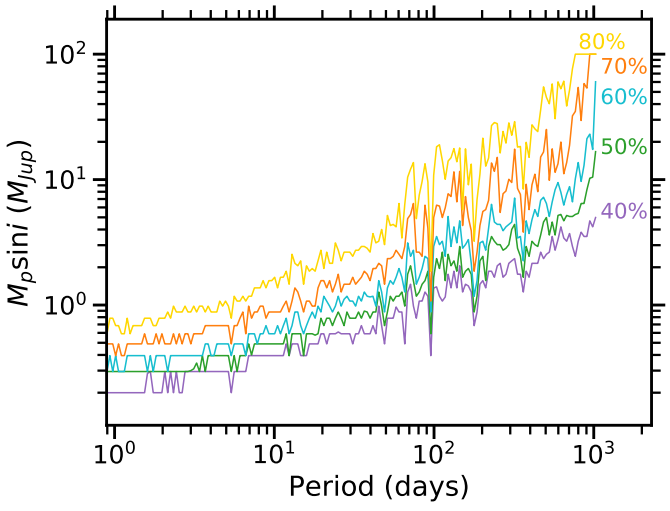

Fig. 12. Search completeness of our survey, corresponding to the lower $m_p \sin i$ for which X% of the star of the survey have detection limits below this $m_p \sin i$ at a given period P. From bottom to top 40–80%.

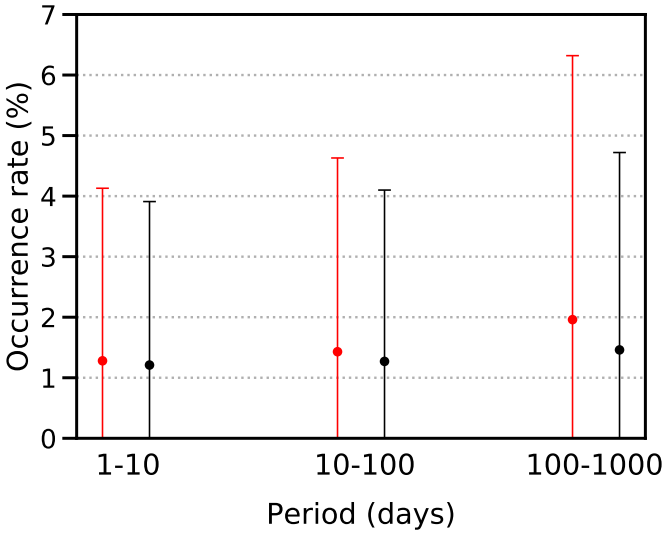

Fig. 13. Upper limits (1σ) on the occurrence rates for our survey for period ranges of 1–10, 10–100, and 100–1000 days in the GP domain (1–13 $M_{\rm Jup}$, red) and BD domain (13–80 $M_{\rm Jup}$, black).

4.6. Comparaison to surveys on main sequence stars

No GP companion with periods lower than 1000 days was detected in the present survey. This non-detection is robust for HJ as 70% of the star of the survey have detection limits lower than 1 $M_{\rm Jup}$ for period lower than 10 days. The completeness of the survey is over 71% for AF and FK stars and

$n_{\rm miss} < 0.4$ for AF and FK stars in the 1–1000 days domain (cf. Table 3). However, we may have missed some planets with low masses and long period as only 40% of the stars of the survey have detection limits lower than $5\,M_{\rm Jup}$ between 100 and 1000 days.

We statistically tested if our GP non-detection implies GP occurrence rates around young stars significantly lower than around older main sequence (MS) stars, using the p-value formalism. The p-value is the probability to get the observed results given a null hypothesis, if it is lower than 10% then the null hypothesis can be rejected. We tested the following null hypothesis: GP occurrence rates are identical around young and main sequence stars in the same mass and period range.

We first applied this formalism in the 1–1000 days domain with a survey that have a completeness similar to ours. For AF MS stars the GP occurrence rate in this domain was estimated at $2.5^{+2.5}_{-0.5}$% (Borgniet et al. 2019). We detected 0 companion out of 23 stars, the corresponding p-value is 56^{+7}_{-21}%. The null hypothesis can not be rejected.

Then, we applied this formalism in the HJ ($P < 10$ days) domain. For FK MS stars, the occurrence rate for HJ in this domain was estimated at: $0.46^{+0.3}_{-0.3}$% by Cumming et al. (2008) and at 1.2 ± 0.38% by Wright et al. (2012). We detected 0 companion out of 52 stars, the corresponding p-value are respectively 79^{+13}_{-11}% and 53^{+12}_{-9}%. The null hypothesis can not be rejected.

There is no evidence for a difference in occurrence rates of HJ between young and MS stars.

BD companions occurrence rates around MS stars is low: $f \leq 1.1^{+4.1}_{-1.1}$% for periods less than 1000 days (Borgniet et al. 2017), our non detection is not surprising. A bigger sample is needed to determine if BD occurrence rates around young and MS stars are different or not.

5. Conclusions

We observed 89 young A- to M-type stars over 3 yr or more with HARPS to search for GP and BD with periods less than 1000 days. This survey allowed to detect close binaries around HD 106906 and around HD 131399 (Lagrange et al. 2015, 2017). We constrained the period of HD 181321B and confirmed the RV trend in HD 186704's RV. We also discovered a low-mass star companion to HIP 36985. No GP companion was detected in this survey. We obtain upper limits on the GP and BD occurrence rates, they are respectively 2^{+3}_{-2}% and 1^{+3}_{-1}% for periods of less than 1000 days. Our comparison of these occurrence rates to those derived for MS stars (Borgniet et al. 2019; Cumming et al. 2008; Wright et al. 2012) indicates that there is no evidence for a difference in occurrence rates of HJ between young and MS stars.

The forthcoming analysis of our SOPHIE survey around young stars and of our on-going HARPS survey on Sco-Cen stars will add 60 and 80 stars, respectively, in our analysis. This will allow for the derivation of more accurate occurrence rates and it will help in the search for the possible impact of system ages on occurrence rates.

Acknowledgements. We acknowledge support from the French CNRS and from the Agence Nationale de la Recherche (ANR grant GIPSE ANR-14-CE33-0018). This work has been supported by a grant from Labex OSUG@2020 (Investissements d'avenir – ANR10 LABX56). These results have made use of the SIMBAD database, operated at the CDS, Strasbourg, France. ESO SD acknowledges the support by INAF/Frontiera through the "Progetti Premiali" funding scheme of the Italian Ministry of Education, University, and Research.

References

Ammler-von Eiff, M., & Guenther, E. W. 2009, A&A, 508, 677
Aumann, H. H. 1985, PASP, 97, 885
Backman, D. E., & Gillett, F. C. 1987, in Cool Stars, Stellar Systems and the Sun, Lecture Notes in Physics, eds. J. L. Linsky, & R. E. Stencel (Berlin: Springer Verlag), 291, 340
Bailey, V., Meshkat, T., Reiter, M., et al. 2014, ApJ, 780, L4
Beichman, C. A., Bryden, G., Stapelfeldt, K. R., et al. 2006, ApJ, 652, 1674
Beust, H., Lagrange-Henri, A. M., Vidal-Madjar, A., & Ferlet, R. 1989, A&A, 223, 304
Bonavita, M., Desidera, S., Thalmann, C., et al. 2016, A&A, 593, A38
Borgniet, S., Lagrange, A. M., Meunier, N., & Galland, F. 2017, A&A, 599, A57
Borgniet, S., Lagrange, A.-M., Meunier, N., et al. 2019, A&A, 621, A87
Bouchy, F., & Sophie Team. 2006, in Tenth Anniversary of 51 Peg-b: Status of and Prospects for Hot Jupiter Studies, eds. L. Arnold, F. Bouchy, & C. Moutou (Paris: Frontier Group), 319
Brandt, T. D., Kuzuhara, M., McElwain, M. W., et al. 2014, ApJ, 786, 1
Carpenter, J. M., Bouwman, J., Mamajek, E. E., et al. 2009, ApJS, 181, 197
Chauvin, G., Desidera, S., Lagrange, A.-M., et al. 2017a, in SF2A-2017: Proceedings of the Annual meeting of the French Society of Astronomy and Astrophysics, ed. C. Reylé, P. Di Matteo, F. Herpin, E. Lagadec, A. Lançon, Z. Meliani, & F. Royer, 331
Chauvin, G., Desidera, S., Lagrange, A.-M., et al. 2017b, A&A, 605, L9
Chen, C. H., Patten, B. M., Werner, M. W., et al. 2005, ApJ, 634, 1372
Chen, C. H., Mittal, T., Kuchner, M., et al. 2014, ApJS, 211, 25
Choquet, E., Perrin, M. D., Chen, C. H., et al. 2016, ApJ, 817, L2
Churcher, L., Wyatt, M., & Smith, R. 2011, MNRAS, 410, 2
Cumming, A., Butler, R. P., Marcy, G. W., et al. 2008, PASP, 120, 531
de la Reza, R., & Pinzón, G. 2004, ApJ, 128, 1812
Delorme, P., Lagrange, A. M., Chauvin, G., et al. 2012, A&A, 539, A72
Delorme, P., Schmidt, T., Bonnefoy, M., et al. 2017, A&A, 608, A79
Desidera, S., Covino, E., Messina, S., et al. 2015, A&A, 573, A126
Desort, M., Lagrange, A. M., Galland, F., Udry, S., & Mayor, M. 2007, A&A, 473, 983
Díez Alonso, E., Caballero, J. A., Montes, D., et al. 2019, A&A, 621, A126
Donaldson, J. K., Roberge, A., Chen, C. H., et al. 2012, ApJ, 753, 147
Donati, J. F., Moutou, C., Malo, L., et al. 2016, Nature, 534, 662
Esposito, M., Guenther, E., Hatzes, A. P., & Hartmann, M. 2006, in Tenth Anniversary of 51 Peg-b: Status of and Prospects for Hot Jupiter Studies, eds. L. Arnold, F. Bouchy, & C. Moutou (Paris: Frontier Group), 127
Figueira, P., Marmier, M., Bonfils, X., et al. 2010, A&A, 513, L8
Folsom, C. P., Bouvier, J., Petit, P., et al. 2018, MNRAS, 474, 4956
Frankowski, A., & Jorissen, A. 2007, Balt. Astron., 16, 104
Fuhrmann, K., Chini, R., Kaderhandt, L., & Chen, Z. 2017, ApJ, 836, 139
Gaia Collaboration (Brown, A. G. A., et al.) 2018, A&A, 616, A1
Galland, F., Lagrange, A. M., Udry, S., et al. 2005a, A&A, 443, 337
Galland, F., Lagrange, A. M., Udry, S., et al. 2005b, A&A, 444, L21
Gallet, F., & Bouvier, J. 2015, A&A, 577, A98
Golimowski, D. A., Krist, J. E., Stapelfeldt, K. R., et al. 2011, AJ, 142, 30
Grandjean, A., Lagrange, A. M., Beust, H., et al. 2019, A&A, 627, L9
Guenther, E. W., & Esposito, E. 2007, ArXiv e-prints [arXiv:astro-ph/0701293]
Hillenbrand, L. A., Carpenter, J. M., Kim, J. S., et al. 2008, ApJ, 677, 630
Hobbs, L. M., Vidal-Madjar, A., Ferlet, R., Albert, C. E., & Gry, C. 1985, ApJ, 293, L29
Holland, W. S., Greaves, J. S., Zuckerman, B., et al. 1998, Nature, 392, 788
Huélamo, N., Figueira, P., Bonfils, X., et al. 2008, A&A, 489, L9
Kalas, P., Liu, M. C., & Matthews, B. C. 2004, Science, 303, 1990
Kiefer, F., Lecavelier des Etangs, A., Boissier, J., et al. 2014, Nature, 514, 462
Kiraga, M. 2012, Acta Astron., 62, 67
Kley, W., & Nelson, R. P. 2012, ARA&A, 50, 211
Koen, C., & Eyer, L. 2002, MNRAS, 331, 45
Kovári, Z., Strassmeier, K., Granzer, T., et al. 2004, A&A, 417, 1047
Lagrange-Henri, A. M., Vidal-Madjar, A., & Ferlet, R. 1988, A&A, 190, 275
Lagrange, A. M., Desort, M., Galland, F., Udry, S., & Mayor, M. 2009a, A&A, 495, 335
Lagrange, A. M., Gratadour, D., Chauvin, G., et al. 2009b, A&A, 493, L21
Lagrange, A. M., De Bondt, K., Meunier, N., et al. 2012, A&A, 542, A18
Lagrange, A.-M., Meunier, N., Chauvin, G., et al. 2013, A&A, 559, A83
Lagrange, A.-M., Mathias, P., & Absil, O. 2015, A&A, submitted
Lagrange, A.-M., Keppler, M., Beust, H., et al. 2017, A&A, 608, L9
Lagrange, A. M., Boccaletti, A., Langlois, M., et al. 2019a, A&A, 621, L8
Lagrange, A. M., Meunier, N., Rubini, P., et al. 2019b, Nat. Astron., 421
Lawler, S. M., Beichman, C. A., Bryden, G., et al. 2009, ApJ, 705, 89
Lindgren, S., & Heiter, U. 2017, A&A, 604, A97

Lo Curto, G., Pepe, F., Avila, G., et al. 2015, The Messenger, 162, 9
Mamajek, E. E. 2012, ApJ, 754, L20
Mamajek, E. E., Meyer, M. R., Hinz, P. M., et al. 2004, ApJ, 612, 496
Mannings, V., & Barlow, M. J. 1998, ApJ, 497, 330
Mayor, M., Pepe, F., Queloz, D., et al. 2003, The Messenger, 114, 2
McDonald, I., Zijlstra, A. A., & Boyer, M. L. 2012, MNRAS, 427, 343
Melo, C., Santos, N. C., Gieren, W., et al. 2007, A&A, 467, 721
Meshkat, T., Bailey, V., Rameau, J., et al. 2013, ApJ, 775, L40
Messina, S., Desidera, S., Turatto, M., Lanzafame, A. C., & Guinan, E. F. 2010, A&A, 520, A15
Messina, S., Millward, M., Buccino, A., et al. 2017, A&A, 600, A83
Meunier, N., Lagrange, A. M., & De Bondt, K. 2012, A&A, 545, A87
Meyer, M. R., Hillenbrand, L. A., Backman, D. E., et al. 2004, ApJS, 154, 422
Meyer, M. R., Hillenbrand, L. A., Backman, D., et al. 2006, PASP, 118, 1690
Meyer, M. R., Carpenter, J. M., Mamajek, E. E., et al. 2008, ApJ, 673, L181
Milli, J., Hibon, P., Christiaens, V., et al. 2017, A&A, 597, L2
Montesinos, B., Eiroa, C., Mora, A., & Merín, B. 2009, A&A, 495, 901
Montet, B. T., Crepp, J. R., Johnson, J. A., Howard, A. W., & Marcy, G. W. 2014, ApJ, 781, 28
Moór, A., Ábrahám, P., Kóspál, A., et al. 2013, ApJ, 775, L51
Morales, F. Y., Bryden, G., Werner, M. W., & Stapelfeldt, K. R. 2016, ApJ, 831, 97
Morin, J., Donati, J. F., Petit, P., et al. 2008, MNRAS, 390, 567
Moro-Martín, A., Marshall, J. P., Kennedy, G., et al. 2015, ApJ, 801, 143
Nidever, D. L., Marcy, G. W., Butler, R. P., Fischer, D. A., & Vogt, S. S. 2002, ApJS, 141, 503
Nielsen, E. L., De Rosa, R. J., Rameau, J., et al. 2017, AJ, 154, 218
Nordström, B., Mayor, M., Andersen, J., et al. 2004, A&A, 418, 989
Olmedo, M., Chávez, M., Bertone, E., & De la Luz, V. 2013, PASP, 125, 1436
Passegger, V. M., Reiners, A., Jeffers, S. V., et al. 2018, A&A, 615, A6
Patel, R. I., Metchev, S. A., & Heinze, A. 2014, ApJS, 212, 10
Paulson, D. B., & Yelda, S. 2006, PASP, 118, 706
Pecaut, M. J., Mamajek, E. E., & Bubar, E. J. 2012, ApJ, 746, 154
Plavchan, P., Werner, M. W., Chen, C. H., et al. 2009, ApJ, 698, 1068
Pollack, J. B., Hubickyj, O., Bodenheimer, P., et al. 1996, Icarus, 124, 62
Poveda, A., Allen, C., Costero, R., Echevarría, J., & Hernández-Alcántara, A. 2009, ApJ, 706, 343
Rameau, J., Chauvin, G., Lagrange, A.-M., et al. 2013a, ApJ, 772, L15
Rameau, J., Chauvin, G., Lagrange, A. M., et al. 2013b, A&A, 553, A60
Rebull, L. M., Stapelfeldt, K. R., Werner, M. W., et al. 2008, ApJ, 681, 1484
Rebull, L. M., Stauffer, J. R., Bouvier, J., et al. 2016, AJ, 152, 114
Rhee, J. H., Song, I., Zuckerman, B., & McElwain, M. 2007, ApJ, 660, 1556
Rodet, L., Beust, H., Bonnefoy, M., et al. 2017, A&A, 602, A12
Schneider, G., Silverstone, M. D., Hines, D. C., et al. 2006, ApJ, 650, 414
Ségransan, D., Mayor, M., Udry, S., et al. 2011, A&A, 535, A54
Sierchio, J. M., Rieke, G. H., Su, K. Y. L., & Gáspár, A. 2014, ApJ, 785, 33
Simon, M., & Schaefer, G. H. 2011, ApJ, 743, 158
Smith, B. A., & Terrile, R. J. 1984, Science, 226, 1421
Soto, M. G., Jenkins, J. S., & Jones, M. I. 2015, MNRAS, 451, 3131
Soummer, R., Perrin, M. D., Pueyo, L., et al. 2014, ApJ, 786, L23
Stauffer, J., Rebull, L., Bouvier, J., et al. 2016, AJ, 152, 115
Strassmeier, K. G., Pichler, T., Weber, M., & Granzer, T. 2003, A&A, 411, 595
Teyssandier, J., Lai, D., & Vick, M. 2019, MNRAS, 486, 2265
Tokovinin, A. 2014, AJ, 147, 87
Tremko, J., Bakos, G. A., Žižňovský, J., & Pribulla, T. 2010, Contrib. Astron. Observ. Skalnate Pleso, 40, 83
van Leeuwen, F. 2007, A&A, 474, 653
Vigan, A., Bonavita, M., Biller, B., et al. 2017, A&A, 603, A3
Wagner, K., Apai, D., Kasper, M., et al. 2016, Science, 353, 673
Weise, P., Launhardt, R., Setiawan, J., & Henning, T. 2010, A&A, 517, A88
Wright, N. J., Drake, J. J., Mamajek, E. E., & Henry, G. W. 2011, ApJ, 743, 48
Wright, J. T., Marcy, G. W., Howard, A. W., et al. 2012, ApJ, 753, 160
Yu, L., Donati, J.-F., Hébrard, E. M., et al. 2017, MNRAS, 467, 1342
Zuckerman, B., & Song, I. 2004, ApJ, 603, 738
Zuckerman, B., Rhee, J. H., Song, I., & Bessell, M. S. 2011, ApJ, 732, 61
Zuckerman, B., Vican, L., Song, I., & Schneider, A. 2013, ApJ, 778, 5

Appendix A: Sample

Table A.1. Stars characteristics for the 89 stars of our HARPS RV survey.

Name HD /BD/CD	HIP	ST	$B-V$	Mass ($M_\odot$)	Age (Myr)	$v \sin i$ (km s^{-1})	Rotation period (days)	IR/D
HD 105	490	G0V	0.600	1.1 [a]	45^{5}_{10} [a]	14.5	–	y [b]/y [b]
HD 984	1134	F7V	0.500	1.2 [a]	42^{8}_{7} [a]	40.0	–	–/n [c]
HD 987	1113	G8V	0.756	0.98 [d]	30^{15}_{15} [c]	7.3	3.72 ± 0.01 [e]	n [f]/y [d]
HD 1466	1481	F8V	0.540	1.2 [a]	45^{5}_{10} [a]	21.0	–	y [g]/y [h]
HD 3221	2729	K4V	1.226	0.9 [e]	45^{5}_{10} [a]	123.0	0.370 ± 0.002 [e]	n [i]/y [h]
HD 6569	5191	K1V	0.830	0.8 [a]	149^{31}_{49} [a]	6.0	7.13 ± 0.05 [e]	–/–
HD 7661	5938	K0V	0.770	–	300^{50}_{50} [c]	7.5	7.46 [j]	n [k]/n [h]
HD 10008	7576	K0V	0.803	0.8 [a]	250^{50}_{50} [a]	3.5	7.15 ± 0.10 [l]	y [m]/y [n]
HD 16765	12 530	F71V	0.520	–	–	32.0	–	–/–
HD 17925	13 402	K1V	0.860	0.9 [a]	150^{150}_{80} [a]	8.5	6.76 [j]	y [o]/–
HD 18599	13 754	K2V	0.880	–	–	4.3	–	–/–
HD 19668	14 684	K0V	0.780	0.9 [a]	149^{31}_{49} [a]	6.5	5.46 ± 0.08 [e]	y [p]/y [c]
HD 24916	18 512	K4V	1.152	0.7 [q]	–	4.5	–	–/–
HD 25457	18 859	F6V	0.500	1.2 [a]	149^{31}_{49} [a]	22.0	3.13 [j]	y [r]/–
HD 26923	19 859	G0IV	0.560	1.07 [q]	–	3.5	–	–/–
HD 29391	21 547	F0IV	0.277	1.75 [s]	37^{9}_{9} [am]	80.0	–	y [n]/–
HD 30447	22 226	F3V	0.390	1.4 [a]	42^{8}_{7} [a]	50.0	–	y [t]/y [u]
HD 35650	25 283	K6V	1.311	0.7 [e]	–	4.0	9.34 ± 0.08 [e]	y [r]/y [v]
HD 37572	26 373	K0V	1.094	0.9 [d]	149^{31}_{49} [a]	9.2	4.52 ± 0.02 [e]	y [r]/n [d]
HD 39060	27 321	A6V	0.170	1.64 [d]	30 [d]	130.0	–	y [w]/y [x]
HD 41593	28 954	K0V	0.825	1.01 [q]	329^{93}_{93} [m]	4.5	–	–/–
HD 43989	30 030	G0V	0.570	1.1 [a]	45^{5}_{10} [a]	45.5	1.15 [j]	y [p]/y [c]
HD 44627	30 034	K1V	0.805	0.9 [e]	30^{15}_{15} [c]	11.5	3.85 ± 0.01 [e]	–/n [c]
HD 45081	29 964	K4V	1.251	0.8 [e]	–	16.4	2.67 ± 0.01 [e]	n [y]/y [c]
HD 45270	30 314	G1V	0.602	1.11 [d]	149^{31}_{49} [a]	17.6	–	y [p]/n [d]
HD 59967	36 515	G3V	0.639	1.09 [m]	353^{58}_{58} [m]	4.0	–	y [m]/–
HD 61005	36 948	G8V	0.740	1.0 [a]	50^{20}_{10} [a]	8.5	5.04 ± 0.03 [aa]	y [ab]/y [ac]
HD 63608	37 923	K0V	0.830	1.0 [a]	250^{50}_{50} [a]	3.2	–	–/–
HD 77825	44 526	K2V	0.992	0.8 [a]	350^{150}_{150} [a]	7.0	8.64 [ad]	–/–
HD 82558	46 816	K1V	0.870	0.8 [ae]	–	29.0	1.70 [j]	–/–
HD 89449	50 564	F6IV	0.440	–	–	16.0	–	–/–

Notes. Spectral type (ST) and $B-V$ values are taken from the CDS database. The $v \sin i$ values are taken from the CDS if present, or are computed with SAFIR based on the CCF width. The IR/D column report if either an IR excess is reported (y) or not (n) and if a disc has been imaged (y) or not (n) in the literature.

References. [a]Vigan et al. (2017), [b]Meyer et al. (2004), [c]Weise et al. (2010), [d]Lagrange et al. (2013), [e]Messina et al. (2010), [f]Rebull et al. (2008), [g]Sierchio et al. (2014), [h]Mamajek et al. (2004), [i]Donaldson et al. (2012), [j]Wright et al. (2011), [k]Lawler et al. (2009), [l]Folsom et al. (2018), [m]Plavchan et al. (2009), [n]Patel et al. (2014), [o]Hillenbrand et al. (2008), [p]Carpenter et al. (2009), [q]Ammler-von Eiff & Guenther (2009), [r]Zuckerman et al. (2011), [s]Simon & Schaefer (2011), [t]Chen et al. (2014), [u]Soummer et al. (2014), [v]Choquet et al. (2016), [w]Aumann (1985), [x]Smith & Terrile (1984), [y]McDonald et al. (2012), [aa]Folsom et al. (2018), [ab]Meyer et al. (2008), [ac]Meyer et al. (2006), [ad]Kiraga (2012), [ae]Kovári et al. (2004), [af]Morales et al. (2016), [ag]Chen et al. (2005), [ah]Golimowski et al. (2011), [ai]Rameau et al. (2013a), [aj]Meshkat et al. (2013), [ak]Rhee et al. (2007), [al]Moór et al. (2013), [am]Montet et al. (2014), [an]Kiraga (2012), [ao]Mannings & Barlow (1998), [ap]de la Reza & Pinzón (2004), [aq]Bailey et al. (2014), [ar]Pecaut et al. (2012), [as]Sierchio et al. (2014), [at]Kalas et al. (2004), [au]Montesinos et al. (2009), [av]Chauvin et al. (2017b), [aw]Nielsen et al. (2017), [ax]Koen & Eyer (2002), [ay]Brandt et al. (2014), [az]Morales et al. (2016), [ba]Strassmeier et al. (2003), [bb]Messina et al. (2017), [bc]Fuhrmann et al. (2017), [bd]Olmedo et al. (2013), [be]Schneider et al. (2006), [bf]Bonavita et al. (2016), [bg]Zuckerman et al. (2013), [bh]Desidera et al. (2015), [bi]Churcher et al. (2011), [bj]Rameau et al. (2013b), [bk]Kalas et al. (2004), [bl]Moro-Martín et al. (2015), [bm]Milli et al. (2017), [bn]Delorme et al. (2017), [bo]Beichman et al. (2006), [bp]Mamajek (2012), [bq]Backman & Gillett (1987), [br]Holland et al. (1998), [bs]Delorme et al. (2012), [bt]Zuckerman & Song (2004), [bu]Lindgren & Heiter (2017), [bv]Passegger et al. (2018), [bw]Poveda et al. (2009), [bx]Morin et al. (2008).

Table A.1. continued.

Name HD /BD/CD	HIP	ST	$B-V$	Mass ($M_\odot$)	Age (Myr)	$v \sin i$ (km s^{-1})	Rotation period (days)	IR/D
HD 90905	51 386	F5V	0.569	1.16 [d]	170^{180}_{70} [a]	10.0	2.60 [j]	y [p]/y [af]
HD 92945	52 462	K1V	0.877	0.9 [a]	170^{130}_{70} [a]	4.0	–	n [ag]/y [ah]
HD 95086	53 524	A8III	0.240	1.6 [ai]	17^{4}_{4} [aj]	22.5	–	y [ak]/y [al]
HD 95650	53 985	M2V	1.477	0.59 [am]	–	11.0	14.80 [an]	–/–
HD 99211	55 705	A7V	0.210	–	–	140.0	–	y [ao]/–
HD 102458	57 524	G4V	0.630	1.70 [ap]	–	31.0	–	y [f]/n [d]
HD 103743	58 241	G4V	0.670	–	–	9.0	–	–/–
HD 105690	59 315	G5V	0.661	1.02 [d]	8^{15}_{8} [c]	8.5	–	–/–
HD 106906	59 960	F5V	0.400	1.5 [aq]	13^{2}_{2} [ar]	55.0	–	y [as]/y [at]
HD 108767	60 965	K0V	−0.050	2.74 [au]	–	6.0	–	–/–
HD 116434	65 426	A2V	0.200	1.96 [av]	14^{4}_{4} [av]	300.0	–	n [av]/–
HD 118100	66 252	K5V	1.180	0.7 [a]	150^{50}_{50} [a]	0.5	3.96 [j]	–/–
HD 131399	72 940	A1V	0.080	2.08 [aw]	21^{4}_{3} [aw]	25.6	–	–/–
HD 141943	–	G2V	0.505	1.09 [d]	30^{15}_{15} [c]	40.0	2.2 [an]	–/n [d]
HD 146464	79 958	K3V	1.033	–	–	17.0	2.329 [ax]	–/–
HD 146624	79 881	A0V	0.022	1.9 [d]	12 [d]	39.0	–	–/n [d]
HD 152555	82 688	F8V	0.600	–	130^{20}_{20} [ay]	10.0	2.77 [j]	n [r]/n [c]
HD 159492	86 305	A5IV	0.189	–	–	54.0	–	–/y [az]
HD 164249	88 399	F6V	0.460	1.3 [a]	24^{5}_{5} [a]	15.0	–	y [t]/–
HD 169178	–	K0V	0.850	–	–	5.5	–	–/–
HD 171488	91 043	G2V	0.551	1.1 [a]	45^{35}_{25} [a]	38.5	1.3371 ± 0.0002 [ba]	–/–
HD 172555	92 024	A7V	0.200	1.61 [d]	12 [bb]	116.5	–	y [d]/y [d]
HD 174429	92 680	G9IV	0.878	1.2 [a]	24^{5}_{5} [a]	69.0	0.944 ± 0.001 [bb]	y [t]/–
HD 177171	93 815	F6V	0.526	1.25 [ap]	30 [d]	300.0	4.737 [ax]	–/n [d]
HD 181321	95 149	G2V	0.630	0.89 [bc]	–	13.0	5.7 [bd]	–/–
HD 181327	95 270	F6V	0.460	1.36 [d]	24^{5}_{5} [a]	19.5	–	y [ao]/y [be]
HD 183414	96 334	G3V	0.650	1.04 [d]	150^{70}_{80} [a]	9.8	3.924 [ax]	–/–
HD 186704	97 255	G0V	0.583	1.4 [bf]	100 [bg]	11.0	3.511 [an]	y [y]/–
HD 188228	98 495	A0V	−0.013	2.03 [e]	40 [d]	85.0	–	–/n [d]
HD 189245	98 470	F7V	0.490	1.2 [a]	150^{150}_{50} [a]	80.0	1.88 ± 0.01 [bh]	–/–
HD 191089	99 273	F5V	0.440	1.3 [a]	24^{5}_{5} [c]	37.3	0.488 ± 0.005 [bh]	y [ao]/y [bi]
HD 197481	102 409	M1V	1.423	0.6 [e]	21^{7}_{5} [ay]	9.6	4.84 ± 0.02 [e]	y [bj]/y [bk]
HD 197890	102 626	K3V	1.053	1.0 [a]	45^{55}_{35} [a]	140.0	0.3804 [an]	y [y]/–
HD 202917	105 388	G7V	0.650	0.9 [a]	45^{5}_{10} [a]	15.4	3.36 ± 0.01 [e]	y [n]/y [u]
HD 206860	107 350	G0V	0.580	1.1 [a]	300^{700}_{100} [a]	12.0	4.86 [j]	y [t]/y [bl]
HD 206893	107 412	F5V	0.440	1.24 [bm]	250^{450}_{200} [bn]	29.0	–	y [as]/y [bm]
HD 207575	107 947	F6V	0.490	1.24 [d]	45^{5}_{15} [a]	30.0	–	y [r]/n [d]
HD 213845	111 449	F7V	0.440	1.4 [a]	250^{750}_{50} [a]	34.0	–	y [bo]/–
HD 215641	112 491	G8V	0.760	–	440^{40}_{40} [ay]	3.6	–	–/–
HD 216956	113 368	A3V	0.090	1.92 [bp]	440^{40}_{40} [bp]	90.0	–	y [bq]/y [br]
HD 217343	113 579	G5V	0.640	1.05 [a]	70 [d]	12.4	–	–/n [d]
HD 217987	114 046	M2V	1.480	0.47 [am]	100 – −10000 [bs]	2.5	–	–/–
HD 218396	114 189	A5V	0.257	1.46 [a]	30 [d]	49.0	–	y [bt]/y [ak]
HD 218860	114 530	G8V	0.738	1.0 [e]	–	6.6	5.17 ± 0.02 [e]	y [r]/–

Table A.1. continued.

Name HD /BD/CD	HIP	ST	$B-V$	Mass ($M_\odot$)	Age (Myr)	$v \sin i$ (km s^{-1})	Rotation period (days)	IR/D
HD 221575	116 258	K2V	0.930	–	–	3.6	–	–/–
HD 223340	–	K1V	0.820	–	–	7.0	–	–/–
HD 224228	118 008	K2V	0.985	0.86 [(d)]	149^{31}_{49} [(a)]	2.6	–	y [(r)]/n [(d)]
–	6276	G9V	0.800	0.9 [(a)]	149^{31}_{49} [(a)]	10.0	6.40 [(j)]	y [(as)]/y [(c)]
–	116 384	K7V	1.347	–	–	4.5	–	–/–
–	17 157	K7V	1.300	–	–	5.0	–	–/–
–	23 309	M0V	1.471	0.55 [(ap)]	10^{3}_{3} [(c)]	5.8	8.60 ± 0.07 [(e)]	–/n [(f)]
–	31 878	K7V	1.296	0.643 [(bu)]	–	5.0	9.06 ± 0.08 [(e)]	–/–
–	36 985	M2V	1.476	0.621 [(bv)]	260^{420}_{260} [(bw)]	5.0	12.16 [(an)]	–/–
–	44 722	K7V	1.450	0.638 [(bu)]	–	9.0	–	–/–
–	46 634	G5V	0.860	–	–	6.0	3.05 ± 0.03 [(e)]	–/–
–	51 317	M2V	1.501	–	130^{40}_{20} [(ay)]	2.6	–	–/–
BD+20 2465	–	M5V	1.300	0.42 [(bx)]	–	3.8	2.60 [(j)]	–/–
CD-46 1064	–	K3V	1.048	0.8 [(a)]	45^{5}_{10} [(a)]	1.0	3.74 ± 0.04 [(e)]	–/–

Table A.2. Results for the 89 stars of our HARPS RV survey.

Stellar characteristics			Survey results.											
Name HD /BD/CD	HIP	ST	TBL	N_m	RV			BVS			RV-BVS corr.	$\langle FWHM \rangle$	$\langle \log R'_{HK} \rangle$	V
					A	rms	$\langle U \rangle$	A	rms	$\langle U \rangle$				
		(day)			(ms^{-1})			(ms^{-1})					(km s^{-1})	
HD 105	490	G0V	4606	36	236.8	61.1	4.2	310.7	9.8	72.9	−0.67	22.6	−4.316	A
HD 984	1134	F7V	867	21	301.9	84.6	16.4	571.8	38.2	137.4	−0.46	59.7	−4.368	A
HD 987	1113	G8V	2621	19	502.6	116.8	2.5	393.6	6.4	103.1	−1.08	13.0	−4.088	A
HD 1466	1481	F8V	4400	19	135.8	39.6	7.4	189.8	17.6	55.9	−0.66	32.3	−4.344	A
HD 3221	2729	K4V	4014	5	4793.4	1794.3	68.6	3115.1	172.5	1447.8	−0.54	203.6	−4.474	–
HD 6569	5191	K1V	8	4	24.0	11.4	1.5	17.8	3.8	7.5	−1.49	9.6	−4.228	A
HD 7661	5938	K0V	1525	29	96.0	28.1	1.2	50.5	3.3	12.5	−1.42	9.2	−4.325	A
HD 10008	7576	K0V	4021	17	20.5	6.2	1.0	17.5	2.7	5.2	0.44	7.5	−4.358	A
HD 16765	12 530	F71V	926	27	173.0	47.2	11.0	402.9	27.9	93.1	−0.42	48.5	−4.475	A
HD 17925	13 402	K1V	1470	40	113.6	30.5	1.1	58.7	3.1	17.4	−0.87	10.0	−4.310	A
HD 18599	13 754	K2V	1055	16	115.9	38.9	1.5	54.3	3.9	17.6	−1.46	9.8	−4.310	A
HD 19668	14 684	K0V	4402	20	143.1	33.2	1.8	91.9	4.7	26.0	−0.95	11.8	−4.284	A
HD 24916	18 512	K4V	792	22	24.3	7.4	0.8	36.7	2.2	11.6	0.46	7.8	−4.536	A
HD 25457	18 859	F6V	4089	78	187.2	49.5	3.3	345.4	7.7	60.2	−0.66	28.2	−4.355	A
HD 26923	19 859	G0IV	4010	47	50.2	12.7	1.1	24.7	3.1	5.6	1.12	8.0	−4.487	A
HD 29391	21 547	F0IV	3996	81	1476.1	326.2	28.4	2564.3	72.1	487.8	–	101.4		P
HD 30447	22 226	F3V	792	19	194.1	47.2	47.7	7048.7	106.6	1728.3	–	120.7	−4.447	P
HD 35650	25 283	K6V	1195	13	48.3	15.3	1.2	43.6	3.0	12.3	−0.67	9.4	−4.359	A
HD 37572	26 373	K0V	2826	34	347.1	75.4	1.7	223.6	4.4	52.8	−1.28	15.6	−4.165	A
HD 39060	27 321	A6V	3702	5108	755.5	341.4	58.9				–			P
HD 41593	28 954	K0V	1194	15	69.5	19.8	1.1	59.4	2.9	16.7	−0.66	9.1	−4.370	A
HD 43989	30 030	G0V	4433	17	819.0	238.6	15.6	743.7	34.3	197.6	−0.83	64.2	−4.209	A

Notes. Spectral type (ST) are taken from the CDS database. The survey results include the time baseline (TBL), the number of computed spectra N_m, the amplitude corresponding to the difference between the maximum and the minimum of the RV(A), rms and mean uncertainty $\langle U \rangle$ on the RV and BVS measurements, the RV−BVS correlation factor (slope of the best linear fit), the mean FWHM ($\langle$FWHM$\rangle$), and the mean $\log R'_{HK}$ ($\langle \log R'_{HK} \rangle$). V stands for the dominant source of RV variations, with A for stellar activity (spots), P for pulsations, B for binary and, T for long-term trend.

Table A.2. continued.

Stellar characteristics			Survey results.											
Name HD /BD/CD	HIP	ST	TBL	N_m	RV			BVS			RV-BVS corr.	$\langle FWHM \rangle$	$\langle \log R'_{HK} \rangle$	V
					A	rms	$\langle U \rangle$	A	rms	$\langle U \rangle$				
		(day)			(ms^{-1})			(ms^{-1})					($km\,s^{-1}$)	
HD 44627	30 034	K1V	4892	23	670.6	177.7	3.2	428.6	8.1	110.9	–	19.1	−4.018	A
HD 45081	29 964	K4V	4020	17	852.4	252.1	5.0	911.0	13.0	246.9	–	24.8	−3.887	A
HD 45270	30 314	G1V	2827	19	137.4	51.8	3.1	193.3	8.4	59.2	−0.76	27.6	−4.335	A
HD 59967	36 515	G3V	1065	25	65.3	19.7	1.4	41.6	3.6	10.5	−0.99	9.0	−4.328	A
HD 61005	36 948	G8V	2369	33	186.5	48.8	2.5	127.4	6.3	32.7	−1.16	14.5	−4.261	A
HD 63608	37 923	K0V	1069	36	80.7	22.2	1.1	49.1	3.0	11.7	−0.63	8.0	−4.323	A
HD 77825	44 526	K2V	283	6	47.0	18.3	1.4	46.5	3.4	14.9	−1.09	9.6	−4.314	A
HD 82558	46 816	K1V	1092	24	296.0	79.7	7.1	475.6	17.5	124.1	−0.43	42.0	−3.990	A
HD 89449	50 564	F6IV	1227	28	129.9	41.4	4.3	351.6	9.1	113.6	−0.26	25.3	−4.971	A
HD 90905	51 386	F5V	2551	24	125.6	40.8	1.9	187.7	5.0	49.0	−0.74	15.0	−4.345	A
HD 92945	52 462	K1V	4533	38	182.3	40.5	1.5	86.2	3.9	23.8	−1.37	10.3	−4.261	A
HD 95086	53 524	A8III	1532	103	1279.0	268.8	14.8	2594.0	36.3	511.1	–	45.4		P
HD 95650	53 985	M2V	4046	12	23.8	7.6	3.1	46.1	7.3	13.6	–	8.0	−4.330	–
HD 99211	55 705	A7V	3068	112	818.0	149.4	86.8	49 704.0	214.7	5222.3	–	183.4		P
HD 102458	57 524	G4V	2964	26	988.5	307.7	10.0	1358.4	23.8	431.7	–	43.6	−3.994	A
HD 103743	58 241	G4V	1065	30	102.2	32.1	2.6	141.6	6.6	35.1	−0.79	14.9	−4.308	A
HD 105690	59 315	G5V	2975	133	269.4	61.3	2.3	193.7	5.4	44.0	−0.91	15.1	−4.276	A
HD 106906	59 960	F5V	1230	46	5290.4	1285.7	32.9	9949.8	83.3	2272.4	–	74.0	−4.574	B
HD 108767	60 965	K0V	1201	18	47.9	12.4	0.7	25.3	2.0	7.7	0.21	8.2	−4.381	A
HD 116434	65 426	A2V	439	58	6273.2	1223.2	1235.6				–			P
HD 118100	66 252	K5V	720	10	534.7	155.6	6.4	139.5	15.6	43.0	−3.48	16.5	−4.108	A
HD 131399	72 940	A1V	189	87	19 478.2	6381.7	16.4	1287.6	39.3	237.0	–	43.1		B
HD 141943	–	G2V	2648	58	861.4	222.8	10.3	1169.7	25.3	269.6	−0.66	53.0	−4.025	A
HD 146464	79 958	K3V	51	5	872.1	352.1	5.0	546.2	12.3	220.6	−1.55	25.8	−4.163	A
HD 146624	79 881	A0V	4762	335	232.7	39.8	29.2	70 472.6	72.9	6163.4	–	65.1		P
HD 152555	82 688	F8V	1135	22	225.0	64.8	6.1	283.2	15.9	69.9	−0.74	26.3	−4.294	A
HD 159492	86 305	A5IV	4751	90	612.4	124.9	20.8	2413.2	52.1	359.7	–	79.4		P
HD 164249	88 399	F6V	1113	25	56.9	14.6	6.9	134.2	17.0	36.7	−0.24	29.8	−4.765	A
HD 169178	–	K0V	1123	19	354.7	135.7	1.8	85.6	4.7	25.0	–	10.7	−4.234	A
HD 171488	91 043	G2V	1111	18	2190.4	717.7	13.1	2249.5	33.2	680.4	−1.0	58.2	−3.988	A
HD 172555	92 024	A7V	2975	262	1883.8	329.6	70.6	94 415.3	185.8	6148.5	–	172.4		P
HD 174429	92 680	G9IV	4572	42	3362.3	970.2	26.0	1167.7	60.0	320.7	−1.77	109.9		A
HD 177171	93 815	F6V	144	21	21 233.2	5931.1	53.4				–		−4.047	B
HD 181321	95 149	G2V	3757	28	2610.2	683.2	3.9	244.0	9.6	59.1	–	19.5	−4.243	B
HD 181327	95 270	F6V	3496	56	63.1	16.3	3.8	156.8	9.0	30.6	−0.26	28.8	−4.577	A
HD 183414	96 334	G3V	3097	68	247.9	63.6	2.4	214.0	6.2	58.3	−1.01	16.0	−4.236	A
HD 186704	97 255	G0V	451	4	345.8	168.8	4.7	77.1	11.9	29.3	–	22.3	−4.308	T
HD 188228	98 495	A0V	4315	194	1398.7	319.2	150.2	211 414.9	368.1	18 294.0	–	148.0		P
HD 189245	98 470	F7V	4285	46	646.2	119.4	21.0	5149.4	43.1	757.5	–	104.2	−4.304	P
HD 191089	99 273	F5V	1025	26	107.1	22.8	15.7	300.0	37.3	78.4	–	57.0	−4.526	P
HD 197481	102 409	M1V	5619	55	667.6	144.0	3.2	470.1	8.0	101.2	−1.37	16.2	−4.289	A
HD 197890	102 626	K3V	13	3	922.1	376.6	85.2	3975.6	217.1	1713.8	–	216.2	−4.277	–
HD 202917	105 388	G7V	4438	20	436.1	124.6	5.0	438.1	12.4	134.8	−0.84	23.0	−3.984	A
HD 206860	107 350	G0V	1332	22	122.1	35.8	2.8	180.9	6.7	51.4	–	16.1	−4.387	A
HD 206893	107 412	F5V	542	15	185.6	45.5	10.8	361.3	21.3	68.2	–	50.7	−4.630	P
HD 207575	107 947	F6V	2391	39	227.6	49.3	9.5	389.5	19.9	97.6	–	49.1	−4.332	P
HD 213845	111 449	F7V	4436	79	220.4	44.2	9.6	454.3	25.8	82.6	–	52.3	−4.703	P
HD 215641	112 491	G8V	1639	78	101.5	20.5	1.2	84.4	3.4	12.2	0.22	8.3	−4.460	A
HD 216956	113 368	A3V	4929	834	382.4	44.3	27.0				–			P
HD 217343	113 579	G5V	2727	26	276.6	96.9	2.7	298.7	6.6	85.6	−1.08	19.3	−4.215	A
HD 217987	114 046	M2V	5109	130	63.8	18.5	0.9	39.5	2.3	8.2	0.95	5.8	−4.899	A
HD 218396	114 189	A5V	2727	124	3616.3	924.5	38.5	7376.0	95.5	2191.3	–	62.3		P
HD 218860	114 530	G8V	1137	18	137.1	36.2	2.1	82.8	5.4	18.6	−1.3	11.7	−4.240	A
HD 221575	116 258	K2V	869	16	45.7	12.2	1.4	33.4	3.7	12.0	−0.54	8.8	−4.438	A

Table A.2. continued.

Stellar characteristics			Survey results.											
Name HD /BD/CD	HIP	ST	TBL	N_m	RV			BVS			RV-BVS corr.	⟨FWHM⟩	⟨log R'_{HK}⟩	V
					A	rms	⟨U⟩	A	rms	⟨U⟩				
		(day)			(ms^{-1})			(ms^{-1})					($km\,s^{-1}$)	
HD 223340	–	K1V	868	10	54.4	17.3	1.7	42.2	4.4	10.7	−1.34	9.8	−4.337	A
HD 224228	118 008	K2V	2815	31	35.4	8.8	1.0	31.5	2.8	7.5	0.32	7.8	−4.356	A
–	6276	G9V	1201	20	95.6	27.3	1.6	91.0	4.2	27.6	−0.65	9.4	−4.321	A
–	116 384	K7V	733	8	104.3	41.2	1.7	60.2	4.5	19.2	−1.18	8.6	−4.455	A
–	17 157	K7V	1457	6	67.5	22.3	1.4	37.1	3.6	14.9	–	8.1	−4.577	A
–	23 309	M0V	4030	16	245.4	64.1	2.3	116.1	5.9	33.0	−1.83	11.7	−3.816	A
–	31 878	K7V	435	11	84.3	31.6	1.6	48.3	4.1	16.1	−1.86	8.5	−4.276	A
–	36 985	M2V	789	20	670.1	247.4	2.1	58.8	5.4	14.7	–	8.1	−4.316	B
–	44 722	K7V	90	4	8.0	3.4	1.5	10.7	3.8	4.0	−0.49	7.6	−4.550	A
–	46 634	G5V	281	3	38.2	16.1	1.4	32.6	3.5	13.9	−1.0	9.8	−4.321	A
–	51 317	M2V	4541	139	17.7	3.6	1.2	24.5	3.2	3.5	−0.38	4.8	−5.032	A
BD+20 2465	–	M5V	3983	40	63.5	16.1	1.2	33.6	3.1	6.5	−0.61	6.7	−4.026	A
CD-46 1064	–	K3V	1185	12	477.8	134.9	8.7	211.2	21.6	68.7	−1.53	17.4	−4.204	A

Appendix B: RV correction from the RV-BVS correlation

Solar to late-type stars present spots on their surfaces. These spots induce a quasi-periodic variations in the line profiles, which cause a signal in the RV and in the BVS. When the lines are resolved, there is at first order a correlation between the RV and the BVS (see Desort et al. 2007 for a detailed analysis).

To correct the RV signal induced by spots, we use Melo et al. (2007) method. It consists in correcting the RV from the linear regression of the RV vs. BVS dataset. The new RV at a given date t is:

$$RV_{corr}(t) = RV(t) - (a * \mathrm{BVS}(t) + b)$$

where a and b are the slope and the intercept of the best linear fit of the RV vs. BVS dataset.

We present in Fig. B.1 an example of such correction for a star with $v \sin i = 31\,km\,s^{-1}$. The mean RV rms of $300\,ms^{-1}$ are reduced to $60\,ms^{-1}$ after correction. This method was used in precedent works that use SAFIR (Lagrange et al. 2013; Borgniet et al. 2017, 2019).

We present a star for which a significant offset due to the HARPS fiber change is present in the corrected RV in Fig. B.2. The initial mean RV rms are $36\,ms^{-1}$. After correction of the offset and of the RV-BVS correlation, the mean RV rms are $10\,ms^{-1}$.

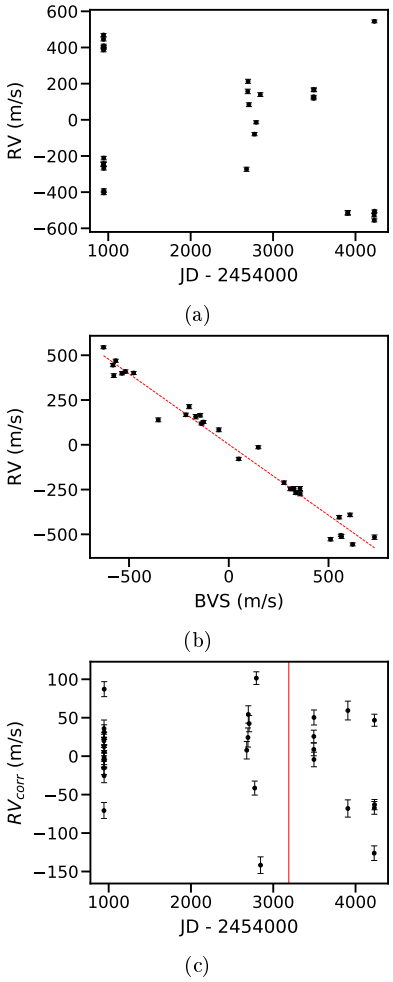

Fig. B.1. HD 102458 RV jitter correction. (*a*) RV time variations. (*b*) RV vs. BVS. The best linear fit is presentend in red dashed line. (*c*) RV corrected from the RV-BVS correlation. HARPS fiber change is shown with a vertical red line.

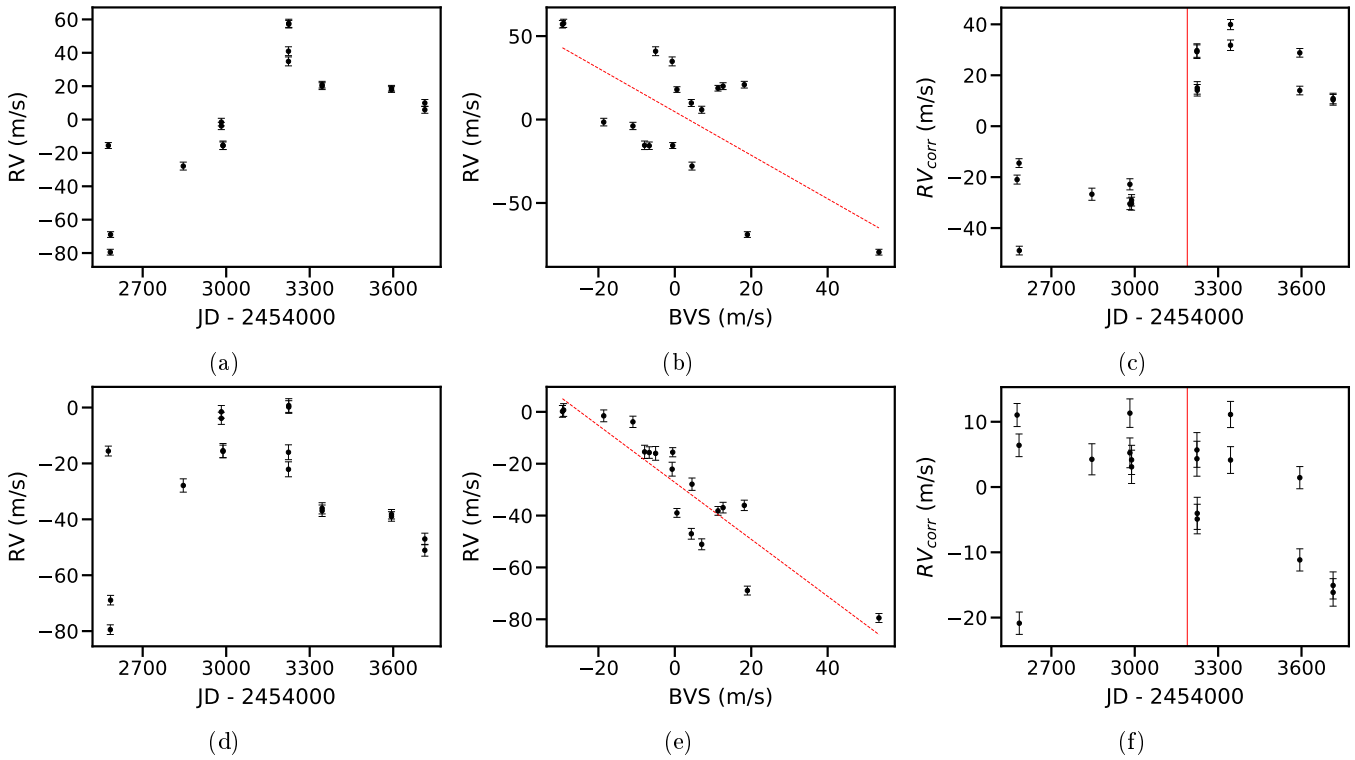

Fig. B.2. HD 218860 jitter and offset correction. (*a*) RV time variations. (*b*) RV vs. BVS. The best linear fit is presented in red dashed line. (*c*) RV corrected from the RV-BVS correlation. HARPS fiber change is shown with a vertical red line. (*d*) RV time variations corrected from the offset due to the HARPS fiber change. (*e*) RV corrected from offset vs. BVS. The best linear fit is presented in red dashed line. (*f*) RV corrected from offset, corrected from their correlation to the BVS. HARPS fiber change is shown with a vertical red line.